



CHALMERS
UNIVERSITY OF TECHNOLOGY

Platicon dynamics in photonic molecules

Downloaded from: <https://research.chalmers.se>, 2026-04-04 16:34 UTC

Citation for the original published paper (version of record):

Rebolledo Salgado, I., Quevedo-Galán, C., Helgason, Ò. et al (2023). Platicon dynamics in photonic molecules. *Communications Physics*, 6(1). <http://dx.doi.org/10.1038/s42005-023-01424-5>

N.B. When citing this work, cite the original published paper.

Platicon dynamics in photonic molecules

Israel Rebolledo-Salgado^{1,2,*}, Clara Quevedo-Galán³, Óskar Bjarki Helgason¹, Anton Lööf¹, Zhichao Ye¹, Fuchuan Lei¹, Jochen Schröder¹, Martin Zelan², and Victor Torres-Company^{1,*}

¹Department of Microtechnology and Nanoscience (MC2), Chalmers University of Technology, SE-412 96 Gothenburg, Sweden

²Measurement Science and Technology, RISE Research Institutes of Sweden, SE-501 15 Borås, Sweden

³CEMDATIC - E.T.S.I. Telecomunicación, Universidad Politécnica de Madrid (UPM), 28040 Madrid, Spain

*israels@chalmers.se

*torresv@chalmers.se

ABSTRACT

Coherent dissipative structures known as platicons can be reliably generated in photonic molecules, resulting in deterministic and reproducible microcombs derived from a continuous-wave pump. However, the supermode spectrum of standard photonic molecules displays numerous avoided mode crossings, distorting the spectral envelope of platicon microcombs. Here, we obtain a platicon microcomb using a photonic molecule configuration based on two coupled microcavities, whose size differs by an order of magnitude. This results in an engineered microcomb spectrum that closely resembles the one generated in an ideal single microresonator with just one frequency mode shift. We observe the coupling between the repetition rate of the platicon microcomb with the frequency of the pump laser, an effect originating from the dispersive-wave recoil induced by mode crossings. Using two identical platicon microcombs, we make use of such coupling to realize dual-comb interferometry. These results contribute to understanding dissipative structures in normal-dispersion microresonators and offer an alternative to applications such as spectroscopy and metrology.

Introduction

Optical frequency combs are coherent light sources whose spectrum consists of an equidistant grid of spectral lines with high phase coherence across the bandwidth^{1,2}. Microresonator-based Kerr frequency combs (microcombs) enable the formation of frequency combs integrated into semiconductor chips^{3,4}. This has driven rapid progress in the understanding of their underlying dynamics and their implementation in practical applications over the last years⁵⁻¹¹. Most of these studies have made use of the high coherence of microcombs achieved through operating in the dissipative soliton regime, utilizing microresonators with anomalous dispersion.

Alternatively, mode-locked soliton microcombs in cavities that yield normal dispersion are of significant interest since obtaining anomalous dispersion in microresonators is challenging. This is due to the fact that many nonlinear materials such as silicon nitride (Si_3N_4) exhibit strong normal dispersion within the visible and near-infrared spectral windows^{12,13}. Therefore, normal dispersion microcombs alleviate the stringent dispersion engineering requirements of the microresonator waveguide^{14,15}. Another important feature of operating in the normal dispersion regime is the high pump-to-comb conversion efficiency offered by mode-locked dark pulses¹⁶⁻¹⁸. Aside from these characteristics, normal dispersion microcombs are particularly appealing towards their foundry deployment since complementary metal-oxide semiconductor (CMOS) waveguides yield normal dispersion^{19,20}. Furthermore, dissipative solitons generated in normal dispersion microresonators exhibit interesting phenomena such as reversible switching of dark-pulse states with pump-laser detuning^{21,22} or supporting bright flat-top pulses called platicons²³.

Nevertheless, comb formation is challenging in normal dispersion cavities pumped with a continuous wave (CW) laser due to the lack of modulation instability (MI). In the absence of MI, it has been proved that microcomb generation is possible using pump modulation schemes²⁴⁻²⁶. Another approach is to pump the microresonator without an optical isolator and then provide feedback to a DFB laser to achieve self-injection locking^{19,24,27}. Moreover, the generation of ideal platicon microcombs can be facilitated if a shift of the pump frequency resonance is present²³.

Such shift of the pump resonance has been successfully implemented using the interaction of an avoided mode crossing (AMC). The presence of AMCs near the pump location is generally thought to prevent the formation of dissipative pulses and

induce instabilities in anomalous dispersion cavities²⁸. In normal dispersion microresonators, the mode coupling between mode families can alter the dispersion locally and create anomalous dispersion bands to attain MI. This mode-coupling interaction was initially explored by the fortuitous mode structure of the microresonator^{29–31}. In recent years, several works have reported the implementation of controllable avoided mode crossing (AMC) by coupling two optical cavities, i.e., a photonic molecule, and producing localized anomalous dispersion^{15,17,32–34}. Similarly, photonic crystal resonators have attracted significant interest to enable phase-matching using an inner periodic structure to shift individual modes of normal dispersion cavities^{35,36}.

In our previous work, we explored the dynamics of dissipative structures in normal dispersion photonic molecules³⁴. The controllable avoided mode crossings facilitate phase matching and enhance the existence range of the solitary waves. However, when the coupled cavities have a similar size, the generated spectra exhibit an asymmetrical distribution influenced by the continuous AMCs^{17,30,34}. In this work, we study a different arrangement inspired by the work in³⁷, where two dissimilar cavities were employed. In this case, the Vernier frequency is much larger, which minimizes the spectral disruptions in our platicon microcomb. The engineered spectrum becomes similar to a single microresonator with an arbitrary frequency shift, constituting an ideal platform to explore the dynamics of platicons, theoretically studied by²³.

Furthermore, we observed that the deviation from this ideal situation, where only one mode is affected, couples the repetition rate of the platicon microcomb with the pump detuning. We support our experimental results with numerical simulations to explain this behavior. This coupling is key for the subsequent realization of dual-comb interferometry, here demonstrated for the first time to the best of our knowledge with normal dispersion microcombs. We show that the stability and coherence of platicon microcombs can be potentially used to perform accurate and ultrafast measurements by retrieving the complex response of a device under test.

Results and discussion

Photonic molecule characterization

In our demonstration, we implement mode-coupling-induced local dispersion using a dual cavity architecture (photonic molecule) to generate the platicon microcomb. The photonic molecule is composed of two linearly coupled cavities, main and auxiliary, with heaters on top, as shown in Figure 1 a. The microresonators of our photonic molecule are fabricated in Si₃N₄ using a subtractive processing method^{38–40}. The optical input power is coupled to the bus waveguide using lensed fibers, and the main cavity is evanescently coupled to a bus waveguide and the auxiliary cavity. The cross-section of the waveguides of both microresonators is 1.6 μm width \times 600 nm height. The fundamental transverse mode of the main cavity operates in the normal dispersion regime. The measured mean intrinsic and extrinsic quality factors of the main cavity are $Q_i = 10.2$ million and $Q_e = 2.6$ million, respectively.

The main cavity has a radius of 455.6 μm , corresponding to a free spectral range (FSR) of 49.97 GHz. In contrast, the auxiliary cavity has a radius of 47.4 μm (FSR of 480.4 GHz), which is one order of magnitude smaller than the main cavity. Consequently, a strong interaction of the avoided mode crossings occurs in a longitudinal mode of the main cavity as illustrated in Figure 1 b. Only a few additional mode crossings are expected within the frequency comb bandwidth span as a result of the FSR's mismatch. These crossings have a minor influence in the comb envelope but, as will illustrate in the next subsection, play a major role in the repetition rate dynamics of the platicons.

The dispersion of the main cavity is characterized using a swept-wavelength interferometry method⁴¹, where the tunable laser is calibrated with the aid of a self-referenced frequency comb⁴². The group velocity dispersion of the main cavity measured near the pump wavelength is 92.4 ps²·km⁻¹. As illustrated in Figure 1 c, the dispersion of the fundamental transverse mode is normal within the C band. The mode coupling between the main and auxiliary resonances leads to avoided mode crossings which in turn causes local perturbations in the dispersion¹⁵. Due to the AMCs, three strong frequency shifts are visible at 1548.59 nm, 1556.63 nm, and 1563.94 nm, which are used to pump the resonator. As can be noticed in Figure 1 c, the avoided mode crossings induced by the auxiliary cavity have a minimal influence on the adjacent resonant modes of the main cavity. This induced frequency shift causes a local change in the dispersion of the modes, yielding anomalous dispersion needed to access modulation instability. This is fundamental for generating parametric gain in the resonator and subsequently initiating the comb formation^{4,43}. The mode interaction, enabled by the presence of the auxiliary cavity, allows for repeatable and deterministic mode-locking associated with the excitation pathway of the dark pulses³⁰. The spectral location of the AMCs can be controlled by applying electrical power to the microheaters. This allows for bringing the avoided resonances closer to each other, offering an extra degree of control in the comb generation.

The photonic molecule chip is placed on a thermal-controlled micro-positioning stage. In order to generate the comb, lensed fibers are coupled to the edges of the chip at the input and output. The coupling losses are 2 dB per facet. The on-chip optical power is 30 mW and is kept fixed throughout the experiments. A wide platicon microcomb is generated and exhibits a power conversion efficiency of 51 percent, where the conversion efficiency is defined as the ratio between the comb power (without pump) and the input power. It is possible to increase the bandwidth of the comb by increasing the input power at the expense of the conversion efficiency. As shown in Figure 1 d, the platicon exhibits the characteristic flat spectral distribution and two

pronounced wings at the edges. Additionally, as mainly one mode interacts with the pump resonance location, the envelope of the microcomb spectrum is highly symmetrical. The repetition rate of the generated microcomb can be directly detected with a photodiode, Figure 1 e shows the beat note and its single side band (SSB) phase noise.

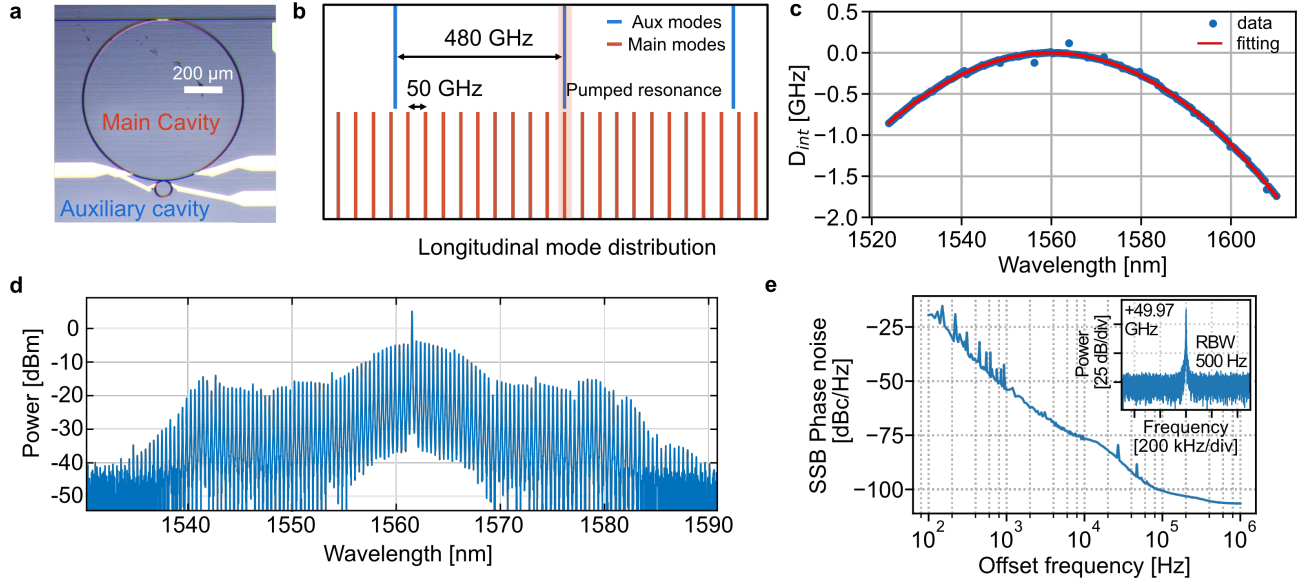


Figure 1. Platicon generation in a photonic molecule. **a)** Microscope picture of the photonic molecule. **b)** Sketch of the longitudinal distribution of the main (orange) and auxiliary cavity modes (blue). **c)** Measured cold cavity dispersion (D_{int}) of the main cavity (blue circles) and a fit of the dispersion profile (red line). **d)** Optical spectrum of the generated platicon microcomb with ~ 50 percent power conversion efficiency with a comb spacing of 49.97 GHz. **e)** Radiofrequency beat note of the repetition rate and single side band (SSB) phase noise of the 50 GHz photodetected signal.

Platicon microcomb states

The platicon microcomb in a photonic molecule is generated by tuning the pump frequency from the blue side towards the red employing the laser piezo using a similar procedure as in³⁴. The initial comb lines are driven by modulation instability followed by Turing rolls spaced by multiple FSRs. Tuning the pump laser further leads to the generation of a comb state with a line spacing of only one FSR and low-amplitude noise. Figure 2 a shows different optical states for different pump frequency offsets. The pump frequency is slowly tuned from an arbitrary point after the soliton regime has been reached. The first stable low-noise platicon state is considered as the reference point (the number I in Figure 2 a and b). The frequency of the pump laser is then tuned in discrete steps while the optical spectrum and the repetition rate are monitored. It can be observed that the bandwidth of the frequency comb increases with the tuning of the pump frequency. The comb states II and III in Figure 2 b exhibit a spectral envelope that closely resembles ideal platons observed in photonic crystals and through self-injection locking generation^{23,27,35}. We note that the change in the bandwidth of the frequency comb is reversible, i.e. decreasing the pump frequency offset induces a reduction of the comb bandwidth. During the tuning between the different states, the comb is coherent. We verified the platicon coherence by monitoring the photo-detected soliton power. The measured radio frequency amplitude noise was at the same level as the pump CW laser, indicating a low noise microcomb state. This process was performed multiple times which indicates that the platicon operation is deterministic.

Another important feature is the reduction and enhancement in power at specific lines of the frequency comb as a function of the pump frequency. This power deviation has been observed in bright solitons where avoided mode crossings modify the phase-matching condition between the pump and cross modes⁴⁴. Similarly, we observe a correlation between the power deviation of the comb lines and the spectral location of the mode crossings, as seen in the upper section of Figure 2 b. The dashed lines correspond to the frequencies where the auxiliary and main cavity modes are predicted to encounter within the central part of the comb. Particularly, around 1563 nm a strong frequency shift caused by the AMC induces the suppression of the comb line power. It can be noticed that the enhancement and suppression of the comb lines' power occur at the AMC's locations when the pump frequency is tuned. Although only five AMC (shaded regions) are shown, this effect appears over twelve crossings that are present within the comb bandwidth. In addition, we observed the typical heightened spectral power at the wings of the platicon, a correspondence to the dispersive wave in normal dispersion microcombs^{45,46}.

Along with the observations on the spectral evolution of the platicon, the repetition rate of the microcomb is monitored. These results are shown in Figure 2 c. The tuning of comb states is encompassed by a change in the repetition rate, which can be controlled by the pump frequency. In these measurements the pump laser is free running without any external feedback control to stabilize the microcombs.

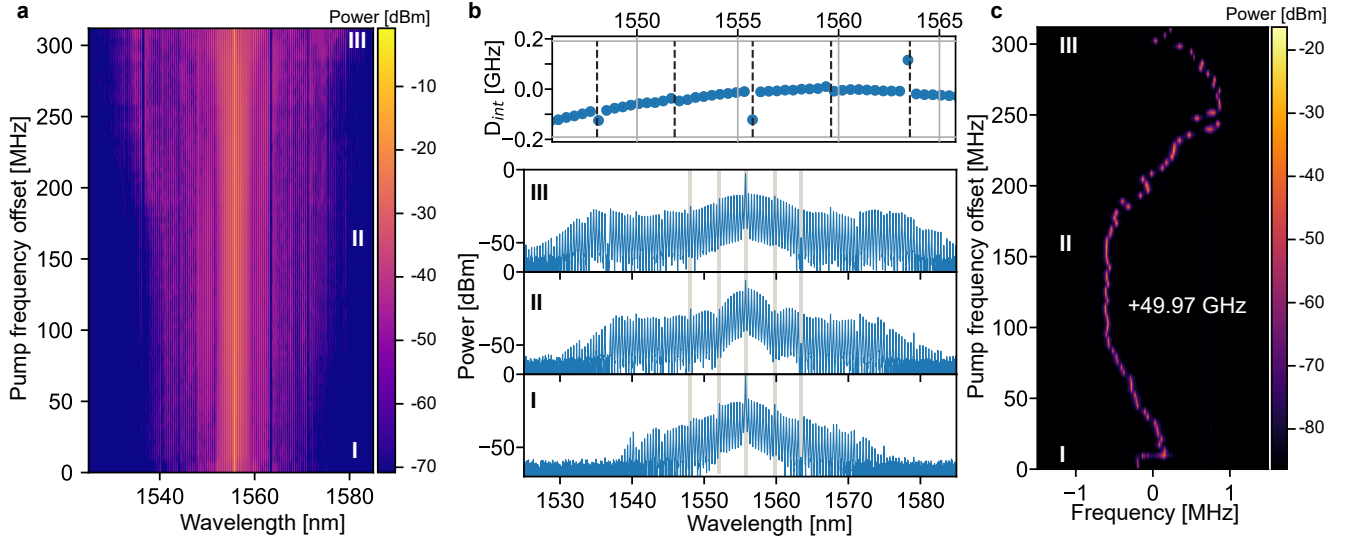


Figure 2. Platicon microcomb evolution as a function of the pump frequency. **a)** Spectral evolution of the frequency comb as a function of the pump frequency, showing multiple platicon states. The first coherent comb state (I) is considered the reference point. **b)** Power deviation of the comb lines located at the mode crossings, identified by the Vernier effect (dashed lines). **c)** Microcomb repetition rate is recorded as the pump frequency is increased, where visible mode crossings are identified by gray shaded lines. A variation in the repetition frequency of the comb is observed.

In order to get a better insight into the repetition rate change, we simulate our experimental findings using an Ikeda map where a mode-coupling-induced shift of the pump mode resonance is considered^{34,47}. Using the parameters retrieved from the cold cavity characterization, we simulated platicon comb structures at different detuning values. The nonlinear Schrödinger equation describes the nonlinear propagation of the field in the microresonator. In our simulations, the platicons are generated starting from a CW pump together with noise-like instead of initial intracavity pulses. Similar to our experiments, we pumped an avoided mode crossing from the blue side, and the detuning parameter evolution is taken into account by linearly tuning the pump frequency location to generate the microcomb. Once the coherent state is reached, the pump detuning is kept constant, and the intra-cavity field converges to a steady state. For the analysis, we calculate the field distribution in the temporal domain, the repetition rate is then attained by monitoring the platicon speed⁴⁸. This process is repeated for different values of the pump frequency shift.

In the simulation, two cases were considered, when only the pump mode is perturbed and when the pump and an additional mode crossing are perturbed, as shown in Figure 3 (a, b), respectively. To implement the AMC, we simulated the interaction of the auxiliary cavity by implementing a constant frequency shift to the main cavity modes³⁷. The magnitude and frequency of the shifts for the pump and additional modes were matched with the parameters measured in the dispersion characterization. When only the pump mode is shifted, the access to anomalous dispersion enables the generation of the dark-pulse structure. In the case where an additional mode is perturbed, a dispersive wave is generated, which causes a spike in the envelope of the spectrum as observed in Figure 3 (b)). Figure 3 (c, d) shows the field distribution upon a frequency scan for both cases. The intra-cavity field is observed in the fast time axis (τ) as the detuning is increased. The plot shows the evolution of the field as it goes through chaotic states and finally enters into a platicon state. When there is no additional mode perturbation, the field distribution propagates in a stable manner (Figure 3 (c)). In contrast, the temporal profile suffers an inclination upon propagation when an additional mode is perturbed and a strong oscillating intracavity background appears (Figure 3 (d)).

This effect has been observed as a consequence of third-order dispersion (TOD) on bright solitons⁴⁹ and employing normal dispersion cavities for platicon formation⁵⁰. In⁵¹, it has been numerically found that both can cause these effects, the presence of AMCs and TOD. However, in our simulations, we have suppressed the TOD, which indicates that the interaction with the mode-crossings causes the long oscillatory tails. This mode-coupling-induced behavior in the normal dispersion is akin to a dispersive wave influenced by third-order dispersion⁴⁵. Moreover, similar results have been observed when using a second coherent pump that is resonant to a mode of the microcavity⁵². This produces the modulation of the field background which

in consequence creates an intracavity potential lattice that traps the soliton stream. Hence, the emission of dispersive waves by means of higher-order dispersion, AMC's, or auxiliary pumping plays a similar role in the stabilization and control of the soliton.

To calculate the repetition rate, the position of the center of mass upon propagation is obtained. Similar to^{47,48}, only the highest intensity part of the waveform is considered so that the background has a minimal influence. It is clear that when only the pump mode is perturbed (an initial requirement for the comb generation) the repetition rate is kept constant (Figure 3 (e)). In the presence of an additional perturbation of one of the modes, the repetition rate varies as the pump frequency is tuned (see Figure 3 (f)). We believe the drift in the platicon velocity is associated with the mode-coupling interaction which causes a shift in the repetition rate. The effect of the additional AMC is twofold. On one hand, it introduces an asymmetry in the microcomb spectrum that shifts its center frequency. This frequency offset will result in a time delay compared to the ideal platicon that arises from the TOD induced by the AMC. The net effect is a coupling between repetition rate and pump frequency⁵³. As the repetition rate is influenced by this velocity drift, it can be tuned in a controllable manner as the pump laser is varied.

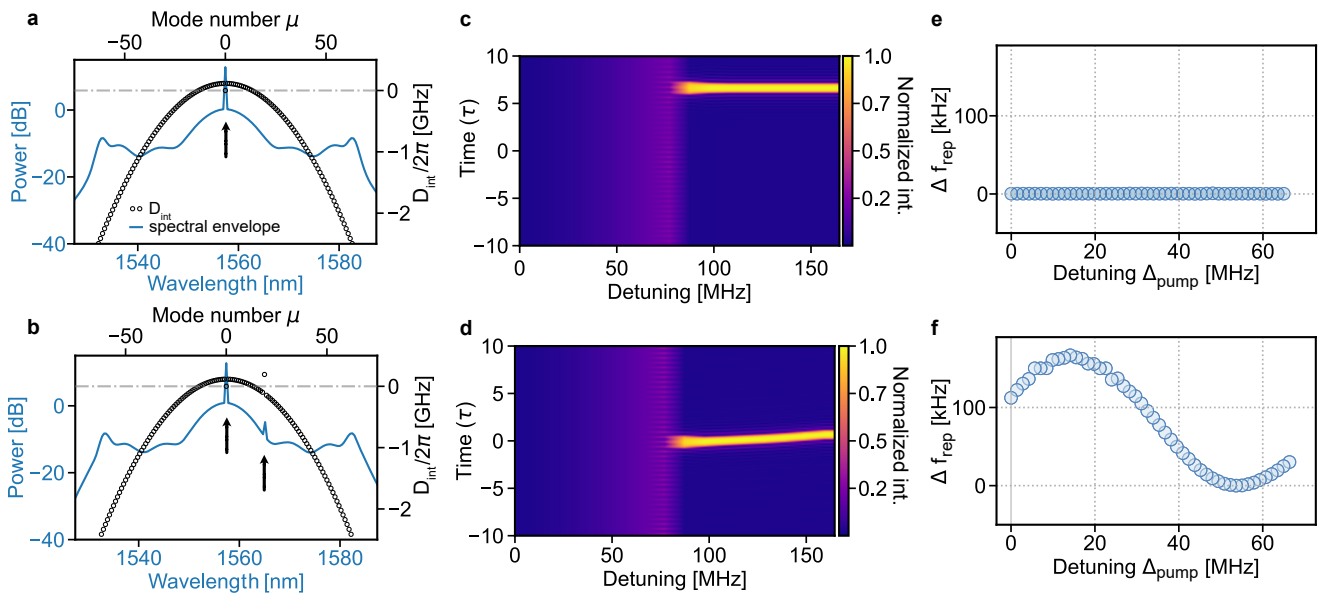


Figure 3. Platicon propagation with different interactions in avoided-mode crossings. **a)** Simulated integrated dispersion profile (empty circles) and optical spectrum (solid line) only perturbing the pump mode and **b)** perturbing the pump mode and an additional mode. **c)** The temporal intra-cavity field distribution as a function of the pump frequency is constant when only the pump mode has been shifted. **d)** A velocity drift is observed with an additional mode crossing induced. **e)** Calculated repetition rate of the frequency comb using the pulse velocity when only the pump mode is shifted and **f)** with a shift in the pump and an additional mode.

Dual-comb interferometry using photonic molecules

The ability to control the repetition rate of the generated microcombs can be very convenient for applications such as dual-comb interferometry (DCI). To demonstrate the capabilities of the platicon microcomb in terms of frequency stability and coherence, we conduct DCI using two photonic molecule microcombs to map the phase response of a device under test (DUT) to the RF domain. For the generation of the two mutually coherent optical frequency combs, two different samples with similar designs are used, which are externally pumped by a single CW laser. Prior to the generation of the combs, the resonances of the microresonators are aligned to the pump wavelength (1555.63 nm) using the microheaters to thermally tune the resonant wavelengths of the main cavities^{17,54}. The maximum frequency shift of the main resonance is $1.75\text{-FSR}_{\text{main}}$ and $0.4\text{-FSR}_{\text{aux}}$ for the auxiliary resonance. Although these shifts are limited by the electrical power that the heater can handle, the pump resonance of the second photonic molecule was shifted by $0.62\text{-FSR}_{\text{main}}$, only a fraction of the maximum shift.

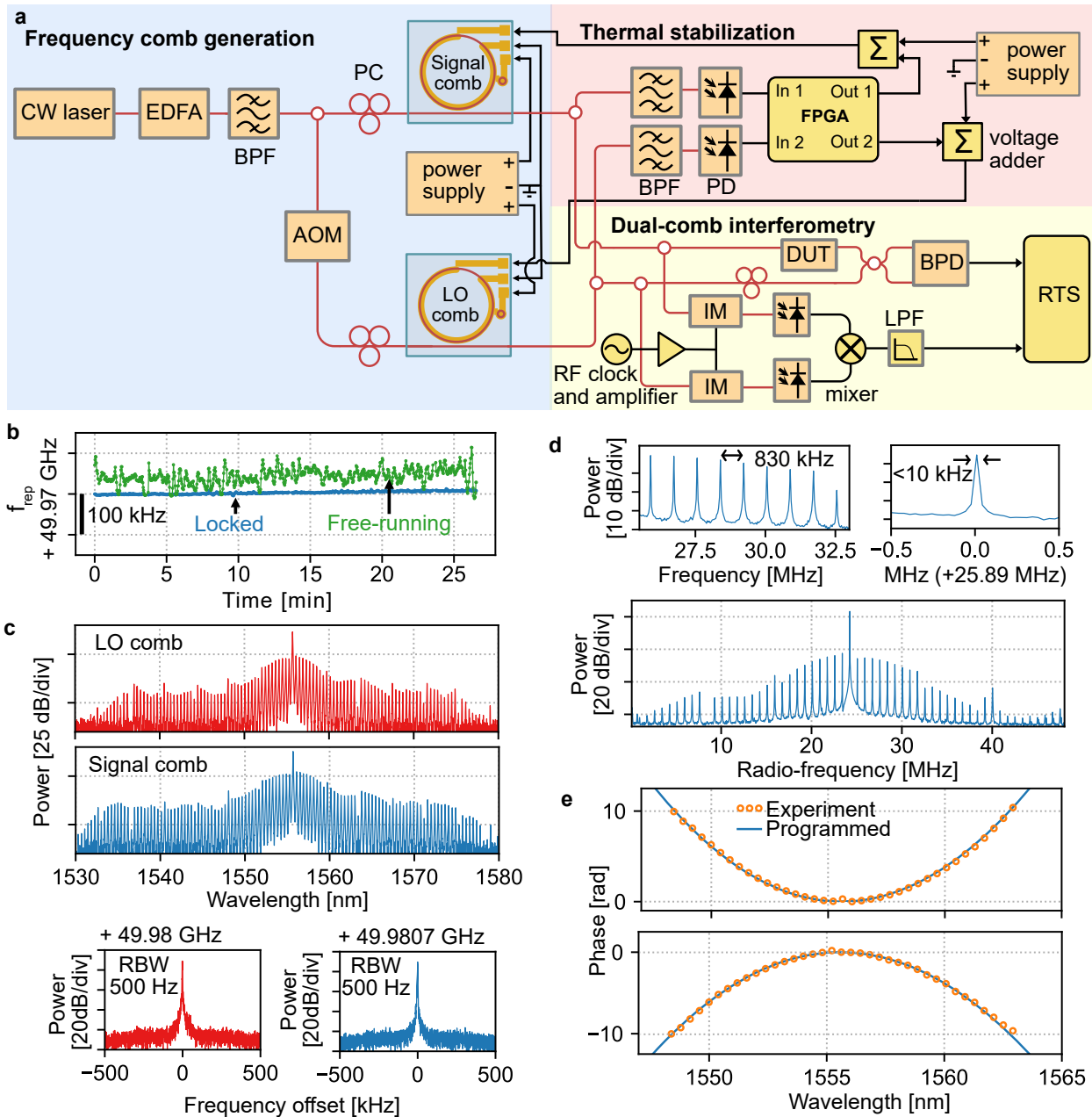


Figure 4. Dual-comb interferometry using platicon microcombs. **a**) Schematic of the experimental setup, in which three blocks can be distinguished. AOM) Acousto-optic modulator, EDFA) Erbium-doped fiber amplifier, PC) Polarization controller, BPF) Band-pass filter, PD) Photodetector, FPGA) Field Programmable Gate Arrays, DUT) Device under test, BPD) Balanced photodetector, LPF) Low-pass filter, IM) Intensity modulator, RF) radio-frequency, RTS) Real-time scope. A main block (blue), where two frequency combs are generated by pumping two photonic molecules with a single CW laser. An AOM is used as a frequency shifter to resolve ambiguous downconversion. A block accounting for the thermal stabilization of the microresonators (red) where a feedback loop is implemented using an FPGA: any thermal drift, that could induce a change in the platicon power, is detected and corrected via a correction signal applied to the voltage control of the microheaters. And a block to perform dual-comb interferometry (yellow) in phase-sensitive configuration and to monitor the repetition frequency difference of both microcombs. **b**) Stability of the repetition rate of one microcomb over time. If the system is free-running, slight environmental changes will cause the repetition rate to drift. **c**) Measured optical spectra of the two platicon microcombs, featuring ≈ 210 comb teeth in a 6 THz span (up), and repetition rate of the microcombs measured with an electrical spectrum analyzer using an electro-optic downconversion technique (low). **d**) RF dual-comb spectrum obtained after performing the Fourier transform of an interferogram trace with an averaging time of 2.1 ms. A zoom of the coherent averaged post-processed spectrum is shown in the upper part with a $\Delta f_{rep} = 830$ kHz. The 3-dB linewidth of the individual RF comb lines is below 10 kHz. **e**) Phase profile of the device under test retrieved through dual-comb interferometry. The blue line corresponds to the phase programmed and the orange dots, to the experimental points.

The experimental setup is shown in Figure 4 a. The CW laser is amplified using an erbium-doped fiber amplifier and divided into two parts to pump the devices. The contribution of the amplified spontaneous emission (ASE) noise to the pump signal is reduced by means of a bandpass filter. An acousto-optic modulator (AOM) with a frequency of 24.3 MHz is used to shift the pump frequency of one photonic molecule in order to avoid ambiguity in the down-conversion process from the optical to the RF domain. To generate the frequency comb in the photonic molecule used as the local oscillator (LO), the CW laser is tuned from the blue to the red-shifted resonance of the avoided mode crossing. Since the pump laser is shared by both devices, the signal comb is generated in the second photonic molecule by finely tuning the resonances of the coupled cavities using the microheaters. After the frequency combs are generated, the comb power is divided into two sections, thermal stabilization, and dual-comb interferometry.

The thermal stabilization is implemented using a proportional-integral-derivative (PID) loop. The input for this control is the photodetected power of the platicon, where a bandpass filter is used to minimize the pump power influence. The correction signal is combined with the DC voltage from a power supply and sent to one of the cavity heaters. In this way, after the platicons are generated, the control signal compensates for any fluctuation and keeps a fixed comb state. Another benefit of this scheme is that is convenient to stabilize the microcomb over time. The platicons were locked to perform the dual-comb measurements, which reduced the broadening of the photodetected comb lines caused by the drifting of the repetition rates. To show the robustness of our system, in Figure 4 b, the repetition rate of the comb was recorded over 30 minutes, where a clear reduction of the drift is observed with a standard deviation of 3.4 kHz and 18.8 kHz for the locked and free-running case, respectively. The two stabilized microcombs are used to perform DCI in a phase-sensitive configuration, and their repetition frequency difference is monitored. Electro-optic intensity modulators are used to down-convert the repetition rate of the LO and signal comb. Both modulators are driven by the same RF oscillator, whose power is amplified in order to have a suitable modulation depth. The difference in repetition rate Δf_{rep} is obtained by mixing the down-converted repetition rates.

The generated frequency combs span an optical bandwidth of ≈ 6 THz (40 nm) around the pump wavelength as shown in Figure 4 c. The repetition rate of both platicons is characterized by electro-optic down-conversion and exhibits a good signal-to-noise ratio. The large SNR of the photodetected signal indicates high stability of both platicon microcombs (see Figure 4 c). To ensure the compression of the dual frequency comb in the first Nyquist zone, the difference in the repetition rate is adjusted by tuning the heater of the main cavity in one photonic molecule. As a result, a rapid thermal drifting over time of the cavity resonances could prevent the mode-locked states of the comb. Furthermore, as the CW laser is free running, its frequency drift could lead to undesirable drift of the detuning. This is overcome by using the thermal-based feedback control described above, using the platicon power to maintain a fixed detuning⁵⁵. Once both frequency combs have reached a mode-locked state and the thermal control is engaged we observed the multiheterodyne beating.

The light coming out of the signal frequency microcomb is sent to a programmable filter where a phase filter is applied^{56,57}. Two filters with an optical bandwidth of 25 nm are programmed, which only modify the spectral phase using a quadratic function with positive and negative signs, respectively. Finally, the signal comb with the encoded phase profile is combined with the LO microcomb using a 50:50 coupler, and the interference signal is then measured using a balanced photodetector and digitized in a real-time sampling scope. As shown in Figure 4 a, the difference in the repetition rate of the microcombs is recorded simultaneously with the interferometric signal. This signal is used as a reference to monitor any drift of the repetition rate caused by the drift of the pump laser. In addition, the reference signal is used in post-processing to extract the individual interferograms from the interferogram trace.

The spectral information is recovered after Fourier analysis of the interferograms. For our measurements, a trace of 2.1 ms containing 1,750 interferograms is used. Figure 4 d shows the obtained RF dual-comb spectrum centered around 24.3 MHz (AOM frequency) and spaced by Δf_{rep} . As shown in the setup, we monitored the drift of Δf_{rep} and calculated a standard deviation equal to 0.73 kHz. The spectral distribution of the RF comb is in qualitative agreement with the optical signal comb. The difference in the line spacing of the combs (see the upper section of Figure 4 d) is $\Delta f_{\text{rep}} = 830$ kHz, leading to a compression factor (defined as the ratio of the repetition frequency and Δf_{rep}) of 6.25×10^4 . As can be noticed, the number of down-sampled lines is smaller than the optical comb, caused by the decreasing power in the comb lines at the edges of the comb. Nevertheless, the quality of the detected beat notes shows a high SNR with a linewidth of 6 kHz. Figure 4 e shows the two spectral phases recovered from the processed dual-comb signals. In the figures, the solid lines correspond to the programmed phase filters and the circles represent the retrieved phase using the dual-comb interferometer. For the computation of the recovered phase, 36 spectral lines around the pump frequency are considered. The excellent agreement between the programmed and the recovered phase with no visible deviations reflects the measurement accuracy of the dual-comb interferometer. We emphasize that in order to benchmark the dual-comb interferometer results, we measured the response of the programmed filter using swept-wavelength interferometry obtaining the same results⁴¹.

Conclusions

In summary, we have demonstrated platicon microcomb generation using modal coupling to induce localized anomalous dispersion in a photonic molecule operating in the normal dispersion regime. We use an architecture where the coupled cavities have highly dissimilar sizes, leading to large Vernier FSR and thus few avoided mode crossings. This reduced interaction between the coupled cavities resonances enables the generation of a microcomb similar to a single resonator with a pump frequency shift. We discovered that the introduction of additional AMCs besides the pump-mode shift couples the repetition rate with the frequency of the pump source. Moreover, we employed this effect to perform dual-comb interferometry using two normal dispersion microcombs.

Methods

Dispersion characterization of the microresonators

The two photonic molecules were characterized using a similar method as in⁴¹, where the dispersion and the linewidth parameters were obtained. The dispersion of the microresonator is described as the resonance frequencies as a function of the mode number⁶, $D_{\text{int}} = \omega_{\mu} - \omega_0 - \mu D_1$, where μ is the mode number with respect of the pump, ω_{μ} are the resonance frequencies. The FSR is $D_1/2\pi$ and the second order dispersion is $D_2/2\pi$. The LO photonic molecule exhibits the following parameters $\text{FSR}_{\text{main}} = 49.99$ GHz, $D_2/2\pi = -1.36$ MHz, $D_3/2\pi = 3.3$ kHz, where $D_3/2\pi$ is the third order dispersion. The intrinsic and extrinsic quality factors are $Q_i = 10.23 \times 10^6$ and $Q_e = 2.56 \times 10^6$. The signal photonic molecule was characterized to have $\text{FSR}_{\text{main}} = 49.99$ GHz, $D_2/2\pi = -1.33$ MHz, $D_3/2\pi = 3.9$ kHz, $Q_i = 13 \times 10^6$ and $Q_e = 2.32 \times 10^6$. Although the dispersion and Q factors were not measured for the auxiliary cavities, we can infer a similar dispersion since the waveguide geometry was the same.

Numerical simulations

The numerical simulations were conducted using the Ikeda map, adding the coupling dynamics of the auxiliary ring similar to³⁴, where a mismatch in the circumference (L) of the ring is considered. The nonlinear propagation in the microresonator driven by the CW laser is described by the nonlinear Schrödinger equation:

$$\left(\frac{\partial}{\partial z} + \frac{\alpha^{(a,b)}}{2} + i\delta^{(a,b)} + d^{(a,b)} \frac{\partial}{\partial T} + i \frac{\beta_2^{(a,b)}}{2} \frac{\partial^2}{\partial T^2} - i\gamma^{(a,b)} |A^{(a,b)}|^2 \right) A^{(a,b)} = 0, \quad (1)$$

where the subscripts a, b correspond to the main and auxiliary cavity, $\alpha^{(a,b)}$ is the propagation loss, $d^{(a,b)}$ describes the pulse walk-off between the two cavities using the main cavity as a reference, $\beta_2^{(a,b)}$ is the group velocity dispersion and $\gamma^{(a,b)}$ is the nonlinear Kerr parameter. The propagation distance is denoted by z , and T is the reference time. At each round-trip, a CW pump together with quantum noise of one photon per spectral bin with random phase is added⁵⁸. The results showed in Figure 3 were obtained by defining the temporal position of the platicon, we use a conventional definition as follows:

$$t_p = \frac{\int t |A(t)|^2 dt}{\int |A(t)|^2 dt}. \quad (2)$$

The parameter $\delta^{(a,b)}$ describes the phase accumulated with respect to the CW laser and used to obtain the pump frequency detuning from the cold-cavity resonance $\Delta f = \text{FSR}^{(a,b)} \delta^{(a,b)} L/2\pi$. Based on the temporal position described above, the repetition rate was calculated for different frequency detuning values.

Thermal stabilization of the photonic molecules

The thermal stabilization system is visualized in Figure 4 a (red shaded block). Both microcombs were stabilized by active feedback control of the detuning. To keep the microcomb state, the detuning is inferred by measuring the platicon power⁵⁵ and controlled by thermally acting on the main cavity. The power supplies are used to tune the spectral separation of the resonances to allow for comb generation and its consecutive control. The control loop consists of a narrow and sharp bandpass filter that selects a portion of the microcomb to measure the converted power. This photodetected power is configured as the set point to create an input signal for the PID controller. The correction signal is then sent to the primary heater power in order to keep the converted power stable.

The control is implemented using a low-cost field-programmable gate array (FPGA) with Python-level functionalities⁵⁹. The photo-detected power of the LO frequency comb (signal) is sent to the fast analog input 1 (input 2), and two independent correction signals are then generated by the FPGA board. Since the analog outputs of the board have a limited voltage level, an operational amplifier is used in a summing configuration where the correction signal and the DC voltage from the power supply

are mixed. The spectrum and the down-converted repetition rate were monitored over a certain time to assess the stability of the thermal control. This control scheme increases the long-term stability of the comb as well as decreases its phase noise within the bandwidth of the controller.

Dual-comb interferometry post-processing

The interference signal obtained at the output of the balanced photodiode is an interferogram whose bursts have a periodicity given by the inverse of the repetition rate of the RF dual frequency comb ($1/\Delta f_{\text{rep}}$). To retrieve the programmed phase profile, two sequential measurements are performed: a calibration measurement to remove the common phase of the interferometer in which a zero-phase filter is applied, and a measurement in which a quadratic phase profile is imparted in the signal microcomb. An additional signal accounting for possible drifts in Δf_{rep} is recorded together with the interferogram to make the post-processing simpler. This signal is generated via electro-optic down-conversion of the repetition rate of both microcombs (see the yellow shaded block in Figure 4 a). The two microcombs are intensity modulated at $f_{\text{mod}} = 25.1$ GHz. For each comb, a beat note from the down-conversion process is detected with a photodetector. The two beat notes are then mixed in an RF mixer generating a sinusoidal signal whose frequency is the repetition rate difference of the two frequency combs.

For our measurements, a temporal trace of duration 2.1 ms containing 1,750 individual interferograms ($\Delta f_{\text{rep}} = 830$ kHz) is digitized at 312 MSa/s. From this signal, 70 sections consisting of 25 interferograms (resolution bandwidth of 32 kHz) are extracted using the zero-crossing points of the reference signal (Δf_{rep}). The Fourier spectra of the interferogram sections are then averaged, reducing the variance of the noise power. To retrieve the phase, a simple peak detection routine is performed to recover the unwrapped phase at the location of the spectral lines. Then, the spectral phases of each interferogram section are averaged. This process is followed for both, the calibration (ϕ_{cal}) and the device under test measurement (ϕ_{DUT}). Finally, the phase response is recovered by subtracting $\phi_{\text{DUT}} - \phi_{\text{cal}}$.

Data availability

The raw data used in this work is available on Zenodo (<https://doi.org/10.5281/zenodo.8380060>).

References

1. Fortier, T. & Baumann, E. 20 years of developments in optical frequency comb technology and applications. *Commun. Phys.* **2**, 153 (2019).
2. Diddams, S. A., Vahala, K. & Udem, T. Optical frequency combs: Coherently uniting the electromagnetic spectrum. *Science* **369**, eaay3676 (2020).
3. Chang, L., Liu, S. & Bowers, J. E. Integrated optical frequency comb technologies. *Nat. Photonics* **16**, 95–108 (2022).
4. Kippenberg, T. J., Gaeta, A. L., Lipson, M. & Gorodetsky, M. L. Dissipative Kerr solitons in optical microresonators. *Science* **361**, eaan8083 (2018).
5. Gaeta, A. L., Lipson, M. & Kippenberg, T. J. Photonic-chip-based frequency combs. *Nat. Photonics* **13**, 158–169 (2019).
6. Herr, T. *et al.* Universal formation dynamics and noise of Kerr-frequency combs in microresonators. *Nat. Photonics* **6**, 480–487 (2012).
7. Marin-Palomo, P. *et al.* Microresonator-based solitons for massively parallel coherent optical communications. *Nature* **546**, 274–279 (2017).
8. Shu, H. *et al.* Microcomb-driven silicon photonic systems. *Nature* **605**, 457–463 (2022).
9. Suh, M.-G. & Vahala, K. J. Soliton microcomb range measurement. *Science* **359**, 884–887 (2018).
10. Spencer, D. T. *et al.* An optical-frequency synthesizer using integrated photonics. *Nature* **557**, 81–85 (2018).
11. Riemensberger, J. *et al.* Massively parallel coherent laser ranging using a soliton microcomb. *Nature* **581**, 164–170 (2020).
12. Moss, D. J., Morandotti, R., Gaeta, A. L. & Lipson, M. New CMOS-compatible platforms based on silicon nitride and hydex for nonlinear optics. *Nat. Photonics* **7**, 597–607 (2013).
13. Xue, X., Qi, M. & Weiner, A. M. Normal-dispersion microresonator Kerr frequency combs. *Nanophotonics* **5**, 244–262 (2016).
14. Fujii, S. & Tanabe, T. Dispersion engineering and measurement of whispering gallery mode microresonator for Kerr frequency comb generation. *Nanophotonics* **9**, 1087–1104 (2020).
15. Xue, X. *et al.* Normal-dispersion microcombs enabled by controllable mode interactions. *Laser & Photonics Rev.* **9**, L23–L28 (2015).

16. Xue, X., Wang, P., Xuan, Y., Qi, M. & Weiner, A. M. Microresonator Kerr frequency combs with high conversion efficiency. *Laser & Photonics Rev.* **11**, 1600276 (2017).
17. Kim, B. Y. *et al.* Turn-key, high-efficiency Kerr comb source. *Opt. Lett.* **44**, 4475–4478 (2019).
18. Wang, C. *et al.* Normal dispersion high conversion efficiency Kerr comb with 50 GHz repetition rate. In *CLEO: Science and Innovations*, SW4N–5 (Optica Publishing Group, 2017).
19. Jin, W. *et al.* Hertz-linewidth semiconductor lasers using CMOS-ready ultra-high-Q microresonators. *Nat. Photonics* **15**, 346–353 (2021).
20. Ji, Q.-X. *et al.* Engineered zero-dispersion microcombs using CMOS-ready photonics. *Optica* **10**, 279–285 (2023).
21. Nazemosadat, E. *et al.* Switching dynamics of dark-pulse Kerr frequency comb states in optical microresonators. *Phys. Rev. A* **103**, 013513 (2021).
22. Parra-Rivas, P., Knobloch, E., Gomila, D. & Gelens, L. Dark solitons in the Lugiato-Lefever equation with normal dispersion. *Phys. Rev. A* **93**, 063839 (2016).
23. Lobanov, V., Lihachev, G., Kippenberg, T. & Gorodetsky, M. Frequency combs and platicons in optical microresonators with normal GVD. *Opt. Express* **23**, 7713–7721 (2015).
24. Liang, W. *et al.* Generation of a coherent near-infrared Kerr frequency comb in a monolithic microresonator with normal GVD. *Opt. Lett.* **39**, 2920–2923 (2014).
25. Liu, H. *et al.* Bright square pulse generation by pump modulation in a normal GVD microresonator. In *CLEO: QELS_Fundamental Science*, FTu3D–3 (Optica Publishing Group, 2017).
26. Lobanov, V. E., Kondratiev, N. M., Shitikov, A. E., Galiev, R. R. & Bilenko, I. A. Generation and dynamics of solitonic pulses due to pump amplitude modulation at normal group-velocity dispersion. *Phys. Rev. A* **100**, 013807 (2019).
27. Lihachev, G. *et al.* Platicon microcomb generation using laser self-injection locking. *Nat. Commun.* **13**, 1771 (2022).
28. Herr, T. *et al.* Mode spectrum and temporal soliton formation in optical microresonators. *Phys. Rev. Lett.* **113**, 123901 (2014).
29. Liu, Y. *et al.* Investigation of mode coupling in normal-dispersion silicon nitride microresonators for Kerr frequency comb generation. *Optica* **1**, 137–144 (2014).
30. Xue, X. *et al.* Mode-locked dark pulse Kerr combs in normal-dispersion microresonators. *Nat. Photonics* **9**, 594–600 (2015).
31. Jang, J. K. *et al.* Dynamics of mode-coupling-induced microresonator frequency combs in normal dispersion. *Opt. Express* **24**, 28794–28803 (2016).
32. Miller, S. A. *et al.* Tunable frequency combs based on dual microring resonators. *Opt. express* **23**, 21527–21540 (2015).
33. Fujii, S. *et al.* Analysis of mode coupling assisted Kerr comb generation in normal dispersion system. *IEEE Photonics J.* **10**, 1–11 (2018).
34. Helgason, Ó. B. *et al.* Dissipative solitons in photonic molecules. *Nat. Photonics* **15**, 305–310 (2021).
35. Yu, S.-P., Lucas, E., Zang, J. & Papp, S. B. A continuum of bright and dark-pulse states in a photonic-crystal resonator. *Nat. Commun.* **13**, 3134 (2022).
36. Yu, S.-P. *et al.* Spontaneous pulse formation in edgeless photonic crystal resonators. *Nat. Photonics* **15**, 461–467 (2021).
37. Helgason, Ó. B. *et al.* Surpassing the nonlinear conversion efficiency of soliton microcombs. *Nat. Photonics*, In Press. (2023).
38. Gondarenko, A., Levy, J. S. & Lipson, M. High confinement micron-scale silicon nitride high-Q ring resonator. *Opt. Express* **17**, 11366–11370 (2009).
39. Ji, X. *et al.* Ultra-low-loss on-chip resonators with sub-milliwatt parametric oscillation threshold. *Optica* **4**, 619–624 (2017).
40. Ye, Z., Twayana, K., Andrekson, P. A. *et al.* High-Q Si₃N₄ microresonators based on a subtractive-Q processing for Kerr nonlinear optics. *Opt. Express* **27**, 35719–35727 (2019).
41. Twayana, K. *et al.* Frequency-comb-calibrated swept-wavelength interferometry. *Opt. Express* **29**, 24363–24372 (2021).
42. Del’Haye, P., Arcizet, O., Gorodetsky, M. L., Holzwarth, R. & Kippenberg, T. J. Frequency comb assisted diode laser spectroscopy for measurement of microcavity dispersion. *Nat. Photonics* **3**, 529–533 (2009).

43. Coen, S. & Haelterman, M. Modulational instability induced by cavity boundary conditions in a normally dispersive optical fiber. *Phys. Rev. Lett.* **79**, 4139 (1997).
44. Lucas, E., Guo, H., Jost, J. D., Karpov, M. & Kippenberg, T. J. Detuning-dependent properties and dispersion-induced instabilities of temporal dissipative Kerr solitons in optical microresonators. *Phys. Rev. A* **95**, 043822 (2017).
45. Cherenkov, A., Lobanov, V. & Gorodetsky, M. Dissipative Kerr solitons and Cherenkov radiation in optical microresonators with third-order dispersion. *Phys. Rev. A* **95**, 033810 (2017).
46. Brasch, V. *et al.* Photonic chip-based optical frequency comb using soliton Cherenkov radiation. *Science* **351**, 357–360 (2016).
47. Lei, F. *et al.* Optical linewidth of soliton microcombs. *Nat. Commun.* **13**, 3161 (2022).
48. Paschotta, R. Noise of mode-locked lasers (part I): numerical model. *Appl. Phys. B* **79**, 153–162 (2004).
49. He, Y., Wang, S. & Zeng, X. Dynamics of dispersive wave emission from dark solitons in Kerr frequency combs. *IEEE Photonics J.* **8**, 1–8 (2016).
50. Lobanov, V. E., Cherenkov, A. V., Shitikov, A. E., Bilenko, I. A. & Gorodetsky, M. L. Dynamics of platicons due to third-order dispersion. *The Eur. Phys. J. D* **71**, 1–5 (2017).
51. Matsko, A. B., Liang, W., Savchenkov, A. A., Eliyahu, D. & Maleki, L. Optical Cherenkov radiation in overmoded microresonators. *Opt. letters* **41**, 2907–2910 (2016).
52. Taheri, H., Matsko, A. B. & Maleki, L. Optical lattice trap for kerr solitons. *The Eur. Phys. J. D* **71**, 1–13 (2017).
53. Yang, Q.-F. *et al.* Dispersive-wave induced noise limits in miniature soliton microwave sources. *Nat. Commun.* **12**, 1–10 (2021).
54. Joshi, C. *et al.* Thermally controlled comb generation and soliton modelocking in microresonators. *Opt. Lett.* **41**, 2565–2568 (2016).
55. Yi, X., Yang, Q.-F., Yang, K. Y. & Vahala, K. Active capture and stabilization of temporal solitons in microresonators. *Opt. Lett.* **41**, 2037–2040 (2016).
56. Durán, V., Tainta, S. & Torres-Company, V. Ultrafast electro-optic dual-comb interferometry. *Opt. Express* **23**, 30557–30569 (2015).
57. Durán, V., Andrekson, P. A. *et al.* Electro-optic dual-comb interferometry over 40 nm bandwidth. *Opt. Lett.* **41**, 4190–4193 (2016).
58. Torres-Company, V., Castelló-Lurbe, D., Silvestre, E. *et al.* Comparative analysis of spectral coherence in microresonator frequency combs. *Opt. Express* **22**, 4678–4691 (2014).
59. Neuhaus, L. *et al.* Pырpl (python red pitaya lockbox)—an open-source software package for FPGA-controlled quantum optics experiments. In *2017 Conference on Lasers and Electro-Optics Europe & European Quantum Electronics Conference (CLEO/Europe-EQEC)*, 1–1 (IEEE, 2017).

Acknowledgments

This work was supported by the European Research Council (GA 771410 DarkComb); Vetenskapsrådet (VR-2020-00453); Stiftelsen för Strategisk Forskning (FID16-0011). C.Q.G. acknowledges support from "Programa Propio UPM" of Universidad Politécnica de Madrid and from grants TED2021-131957B-100 and PID2021-1234590B-C21 funded by MCIN/AEI/10.13039/501100011033 and by the European Union NextGeneration EU/PRTR and ERDF "A way of making Europe". The Si₃N₄ devices were fabricated at Myfab Chalmers.

Author contributions

I.R.S. conducted the experiments with the assistance of C.Q.G. and A. L. and the numerical simulations with assistance from F.L. O.B.H. designed and characterized the samples. Z.Y. fabricated the samples. I.R.S., C.Q.G., O.B.H., F.L., and V.T.C. analyzed the data and discussed the results. I.R.S., C.Q.G., M.Z., and V.T.C. prepared the manuscript with input from the co-authors. V.T.C. supervised the project with the input of J.S. and M.Z.

Competing interests

V.T.C. is a Guest Editor of the Collection 'Microresonator Frequency Combs: New Horizons' for Communications Physics, but was not involved in the editorial review of, or the decision to publish this article. Others declare no competing interests.